Desalination and Water Treatment
www.deswater.com

doi: 10.5004/dwt.2020.25735

191 (2020) 426–437
July

Tiger nut residue as a renewable adsorbent for methylene blue removal from solution: adsorption kinetics, isotherm, and thermodynamic studies

Alexander Nti Kani, Evans Dovi, Farid Mzee Mpatani, Zhaohui Li*, Runping Han*, Lingbo Qu*

Henan Joint International Research Laboratory of Green Construction of Functional Molecules and their Bioanalytical Applications, College of Chemistry, Zhengzhou University, No 100 of Kexue Road, Zhengzhou 450001, China, Tel. +86 371 67781757; Fax: +86 371 67781556; emails: zhaohui.li@zzu.edu.cn (Z. Li), rphan67@zzu.edu.cn (R. Han), qulingbo@zzu.edu.cn (L. Qu), mykani@yahoo.com (A. Nti Kani), evansdovy@gmail.com (E. Dovi), papilampatani@gmail.com (F. Mpatani)

Received 24 September 2019; Accepted 21 February 2020

ABSTRACT

Tiger nut residue (TNR), an agricultural waste, was investigated as a cheap and eco-friendly adsorbent to remove methylene blue (MB) from solution. The surface characteristics of TNR were analyzed by X-ray diffraction, Fourier transform infrared spectroscopy and scanning electron microscopy. The results showed that increasing dose resulted in increased percentage removal. TNR had a pH_{zpc} of 5.5. The presence of salt in the system did not significantly affect MB removal. Higher temperatures were not beneficial to the adsorption process. The adsorption mechanism is predicted by the pseudo-second-order kinetic model while Langmuir and Freundlich's equations describe best the adsorption isotherm. The maximum adsorption capacity by Langmuir isotherm is 146 mg/g. Thermodynamic analyses suggested that MB adsorption onto TNR was a physisorption process that was spontaneous and exothermic and that no remarkable change in entropy occurred during the adsorption process. Finally, the cost analysis was presented. The potential of TNR to be used as the future of green and sustainable adsorbent has been further demonstrated by its potent reusability.

Keywords: Tiger nut residue; Batch adsorption; Methylene blue; Kinetics; Isotherm

1. Introduction

Rapid global industrial revolution coupled with the high rate of population growth has resulted in the pollution of global water resources [1,2]. Water pollution has since become an important issue of environmental concern worldwide [3]. The various hazardous pollutants, including dyes, released into these water bodies are mostly of organic and inorganic sources [4]. Dyes are categorized into two main groups: natural and synthetic [5]. Synthetic dyes are also divided into three groups: anionic (direct, acid, and reactive dyes), cationic (basic dyes) and non-ionic dyes (disperse and vat dyes) [2]. The dye molecules present in the wastewater are problematic because of their high molecular stability, poor biodegradation, carcinogenic and mutagenic effects to both aquatic fauna and human beings. Besides, they are not only aesthetically displeasing but also toxic to aquatic life because of their ability to decrease sunlight penetration into the water, thus reducing the photosynthetic activity of the systems [2,6]. Sources of these dyes include textile, food, cosmetics, pharmaceutical industries, and health facilities [4,6]. These dyes are applied as colorants, in foods, paint, textiles, cosmetics, leather, paper-making, plastics, and stains in the health and pharmaceutical industries [5]. Ranjith et al. [2] indicated that cationic dyes are more toxic and higher in tinctorial values than anionic dyes. Among these cationic dyes, methylene blue (MB) is the most commonly used dye for several purposes as stain,

* Corresponding authors.

dermatological agent, additive to poultry feed, paper industries, and extensively used in textiles. MB dyes are non-biodegradable, toxic, cause allergy and carcinogenic to human beings. MB has a maximum absorption peak at a wavelength of 665 nm, a molecular formula of $C_{16}H_{18}ClN_3S$, with a molar mass of 319.85 [7]. Therefore, for the sake of human health and ecological security, it is impending to take measures to reduce the degree of damage [8] and even achieve a risk-free level from dye pollution in our environment [5]. Researchers have explored several technologies and methods to address this menace. These include photocatalysis, electrochemical oxidation, ozone treatment, membrane separation, flocculation, coagulation, oxidation, biological methods and precipitation for the removal and purification of dye wastewater [1,2,4,6]. However, these methods present some disadvantages related to the high cost of operation and production of secondary pollutants.

Adsorption is a promising technique in dye removal. It is efficient, versatile, simple in design, eco-friendly, low in cost, and widely used color removing technique [3]. Zhang et al. [8] acknowledged this fact as they posit that adsorption technology is gaining significance in fundamental studies and industrial applications. Some of the reported materials that have been studied in environmental dye pollutant treatment include clay materials, chitosan, double-layered hydroxides, fly ash, activated carbon, resin, biological straw, carbon nanotubes among others [2,4–6,8,9]. Good performance of adsorption materials plays a vital role in wastewater purification [5]. Cellulose is one of the most abundant biomacromolecules in nature which is very degradable and a nontoxic potential candidate for use as an adsorbent in dye removal [10].

Plant cell walls are made up of cellulose, hence their potential use as adsorbents is worth investigating. Recently, the use of agricultural waste as alternative classical adsorbents have been reported. Raw and modified almond shells have been used for the removal of methyl violet 2B [11] and crystal violet [12] from aqueous solution. In other related dye adsorption studies, MB was removed from aqueous solution by peanut husk [13], phoenix tree's leaves [14] and cereal chaff [15] in batch and fixed-bed column modes. The low adsorption capacities reported by these studies motivated us to investigate the use of *Cyperus esculentus* as an adsorbent since there is no report of its usage in dye removal at present.

Cyperus esculentus (also called tiger nut sedge, chufa sedge or earth almond) is a crop of the sedge family widespread across much of the world and widely cultivated for its edible tubers. It is found in most of the Eastern Hemisphere including Africa, Southern Europe, and Madagascar, as well as the Middle East and the Indian subcontinent. This herb grows and reproduces quickly. Its tubers can develop in soil depths around 30 cm, but most occur in the top or upper part. They tolerate many adverse soil conditions including periods of drought and flooding and can survive soil temperatures around –5°C [16]. Tiger nut residue (TNR), thus, presents us with a 'green', eco-friendly, easily accessible, and economically potential alternative adsorbent.

This study aims to use TNR as a 'green', eco-friendly and low-cost absorbent material to efficiently remove MB from solution. The effect of pH and salt concentration on adsorption as well as the isotherm, kinetics, and thermodynamic parameters were also investigated.

2. Materials and methods

2.1. Chemicals and materials

MB was purchased from Shanghai Lanji Technology Development Co., Ltd., (Shanghai, China). Absolute ethanol (EtOH) was bought from Fuchen Chemical Reagent, (Tianjin, China). Sodium chloride (NaCl), sodium hydroxide (NaOH) and calcium chloride ($CaCl_2$) were obtained from Zhengzhou Chemical Corporation, (China). All the chemicals used in this study were of analytical grade hence they were used without further purification. TNR was collected from a tiger nut milk-producing shop in Bantama Market in Kumasi, Ghana. It was washed extensively with tap water and filtered to obtain the residue. The collected TNR was then dried in an oven at 60°C until a constant weight was obtained. The dried TNR was sieved to produce particles of 40–60 mesh.

2.2. Preparation of MB solutions

A standard solution (1,000 mg/L) of MB was prepared by dissolving a precisely weighed amount of MB in a known volume of distilled water. The other experimental solutions were prepared by diluting the standard solution of MB with distilled water to give a suitable concentration and the pH (2–13) was varied using 1 mol/L NaOH or HCl solution.

2.3. Characterization

The crystal structure of the TNR was examined using X-ray diffraction (XRD) (PANalytical, Netherlands). TNR and TNR@MB pore volume, pore size and specific surface area were evaluated based on the Brunauer–Emmett–Teller method (BET, ASAP2420-4MP, American). The characteristic functional groups were determined using Fourier transform infrared spectroscopy (FTIR Spectrometer, Nicolet iS50, American). The surface was imaged using scanning electron microscopy (SEM) (JSM-7500F cold field emission scanning electron microscopy). The pH_{zpc} (pH zero point charge) of adsorbent was carried out following the method described by Meili et al. [7] with some modification. Briefly, the initial pH (pH_i) of 10 mL of distilled water in a 50 mL conical flask was adjusted from pH of 2–13 using few drops of 0.10 mol/L of HCl or 0.10 mol/L of NaOH solution. 20 mL of 0.05 mol/L of NaCl solution was then added to each conical flask containing the pH adjusted distilled water. The adsorbent was then added to conical flasks containing adjusted pH solutions. The adsorbent solutions were then equilibrated in the shaker for 24 h at 120 rpm and 30°C. The suspensions were filtered and the final pH (pH_f) was recorded. The change in solution pH ($\Delta pH = pH_f - pH_i$) was calculated for each solution, and a plot of ΔpH vs. initial pH (pH_i) was sketched to determine the value of pH_{zpc}.

2.4. Adsorption experiments

The removal of MB from aqueous solution by TNR was studied in batch mode. A certain amount of adsorbent was added to a 50 ml conical flask, and then 10 mL of MB solution

was added. The effect of pH, contact time, temperature, concentration, adsorbent dose, and salt were investigated to study the effect of the operational parameters on the removal of the dye from the solution. Then the conical flasks were placed in a thermostatic shaker (Kexi Instrument KW-1000DB, China) at 120 rpm at a constant temperature for a given time. After adsorption, TNR was separated from the solution by centrifugation at 3,000 rpm and MB concentration was measured. Visible spectrophotometry (Persee TU-1900, China) was used for the analysis of MB at a maximum absorption wavelength of 665 nm. The spectra (obtained from the instrument) of dye before and after adsorption is shown in Fig. 1. All experiments were performed in triplicate to ensure accuracy, reproducibility, and the average ($n = 3$) results were used for further data analysis using Microsoft Excel 2016 version and Origin 8.5.

The adsorption capacity (q) and removal efficiency (% p) of the TNR to MB were calculated in the light of Eqs. (1) and (2):

$$q = \frac{V(C_0 - C)}{m} \tag{1}$$

$$p = \frac{(C_0 - C)}{C_0} \times 100\% \tag{2}$$

where C_0 and C are the initial and equilibrium concentration or concentration at any time t (mg/L) of MB, V is the volume (L) of MB and m is the mass (g) of TNR.

2.5. Desorption and regeneration study

The MB-loaded TNR (TNR@MB) was obtained for MB adsorption at an initial concentration of 100 mg/L (pH 4.0) at 30°C and the first-time adsorption quantity q_e was calculated. Then, TNR@MB was washed with distilled water to remove the unabsorbed dye and was dried at 60°C in an oven. The exhausted TNR was regenerated by several solutions including ethanol, 75% ethanol, 0.16 mol/L NaCl, 0.010 mol/L NaOH and 1% HCl (pH = 1) solution. However, the best method (75% ethanol) was used for multiple desorptions and regeneration studies. 10 mL of 75% ethanol was mixed with the TNR@MB into a conical flask and oscillated at 30°C to obtain equilibrium, then the concentration of the supernatant was measured. The regenerated adsorbent was reused at the same experimental conditions. The regeneration yield was obtained as the ratio of values of q_e before and after regeneration.

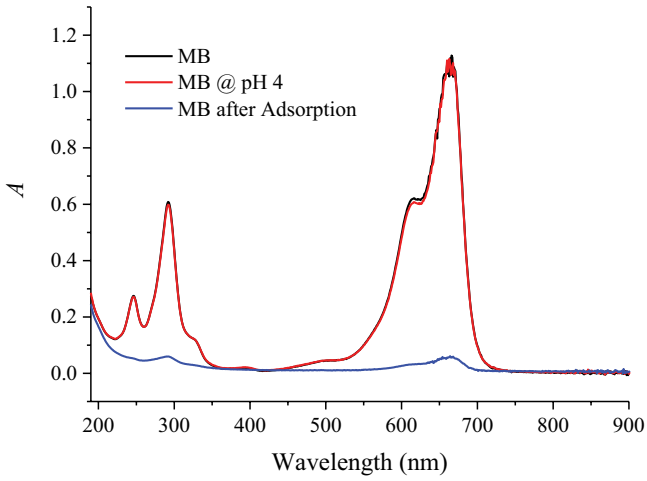

Fig. 1. Spectra of maximum absorption wavelength of MB and MB working solution before and after adsorption.

3. Results and discussion

3.1. Characterization of adsorbents

3.1.1. pH point of zero charge (pH_{zpc})

The point of zero charge is the pH at which the surface of the adsorbent is globally neutral. It describes the condition when the electrical charge density on a surface of the absorbent is zero [17]. It determines how easily a substrate is able to adsorb potentially harmful ions. Hence it is indispensable to measure pH_{zpc} of TNR. The results are shown in Fig. 2. It was seen from Fig. 2 that the pH_{zpc} was 5.5. Below this value, the surface is positively charged whiles beyond this value, it is negatively charged. Therefore, it was expected that adsorption takes place at pH higher than 5.5 since MB is a cationic dye, however, adsorption had reached over 90% at pH 4 (acidic). Thus, TNR is a novel adsorbent to efficiently remove MB over a wide range of pH.

3.1.2. FTIR analysis

The FTIR analysis was performed to study the surface chemistry of TNR and TNR@MB between the range of 4,000–500 cm^{-1} since it is an important tool to identify some important functional groups, which are capable of adsorbing pollutants [13]. Fig. 3 presents the FTIR spectrum of the adsorbent before and after adsorption.

From Fig. 3, no obvious changes in the bands were observed on the studied materials (TNR and TNR@MB). The structure and composition of TNR were complex. The strong peak at 34,421 cm^{-1} is assigned to stretching and bending vibration of –OH functional group and molecular H_2O [5] which indicates a significant hydrogen-bond interaction [18].

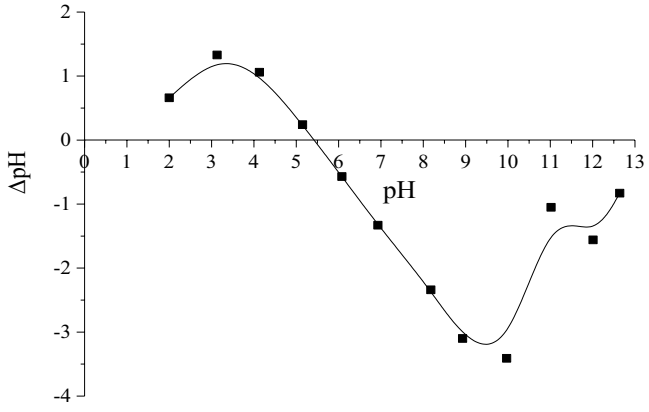

Fig. 2. Point of zero charge of TNR (pH_{pzc} 5.5).

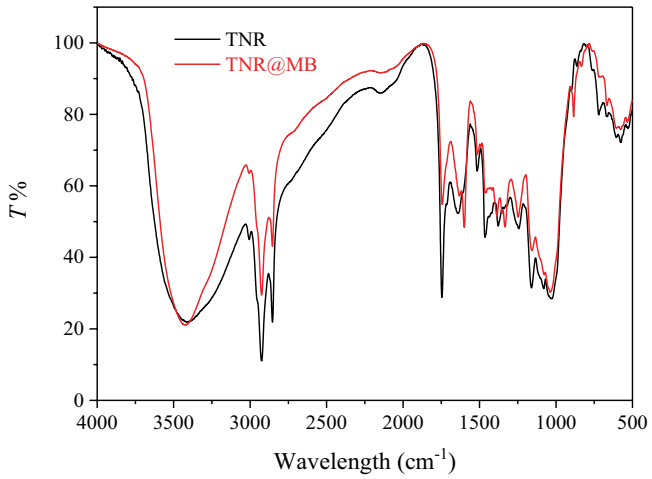

Fig. 3. FTIR spectra of TNR and TNR@MB.

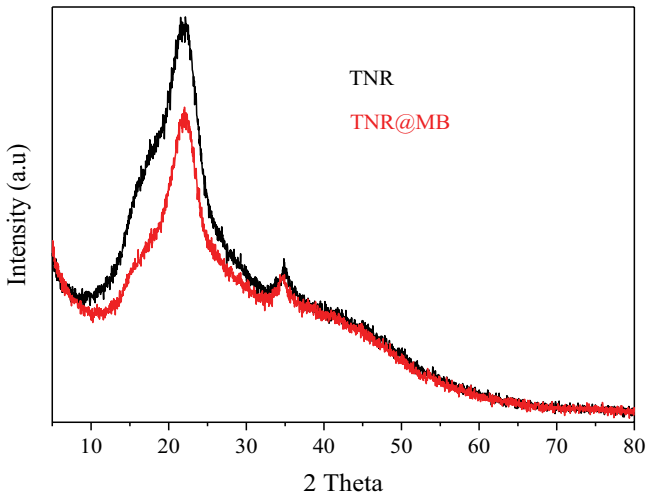

Fig. 4. XRD patterns of TNR and TNR@MB.

The bands at 2,924 and 2,853 cm^{-1} are the vibration peaks of $–CH_3$ and $–CH_2$ groups [19]. The bands at 1,740 cm^{-1} indicates the stretching vibration of C=O, and the bands at 1,515 cm^{-1} denotes the in-plane vibration of C=C due to the aromatic ring vibration of lignin in TNR [20]. The band at 1,639 cm^{-1} is attributed to the presence of carbonyl (C=O) functional groups and the band at 1,080 cm^{-1} denotes the deformation vibrations of C–O [21]. In addition, the bands at 1,464; 1,380; and 1,242 cm^{-1} are assigned to the bending vibration of the $–CH_2–$, the deformation vibration of $–CH_3–$ in cellulose, and the vibration of the C–O [22]. The absorption band, indicative of alcohols –OH and aliphatic ethers (C–O–C) (1,160–1,026 cm^{-1}), is related to oxygenated functional groups in cellulose [18]. These bands above are the adsorption bands that all plant-based materials contain. Comparison FTIR of TNR and TNR@MB, it is observed that the location of the main peak was not significantly changed, but the strength of peaks at 1,740 and 1,242 cm^{-1} decreased, which suggests that functional groups containing oxygen played an important role during MB adsorption.

The percentage composition of carbon, hydrogen, and oxygen in the TNR were 49.28%, 6.06%, and 44.66%, respectively. The results show that there are polar functional groups containing oxygen which are in favor of adsorption.

3.1.3. XRD analysis

XRD pattern is mainly used for crystal structure analysis. The XRD pattern of TNR and TNR@MB are presented in Fig. 4. The characteristic diffraction peak at 22.57° and 34.27° correspond to planes (200) and (004) indicative of the presence of highly organized crystalline cellulose [23,24]. There was no obvious difference between the XRD patterns of TNR and TNR@MB, which indicated that MB had no effect on the graphitic nature of the TNR [9].

3.1.4. BET analysis

The investigation of specific surface areas and total pore volumes of the adsorbent before and after adsorption are shown in Table 1. The results indicate the poor porosity of the adsorbent. It is observed that the adsorption of MB by TNR increases both the BET surface area and the total pore volume. However, the BET pore size decreases from 3.41899 to 3.14962 nm. This may be as a result of the partial blockage of the pores by MB molecules [25].

Table 1
BET analysis of TNR and TNR@MB

Textural properties	TNR	TNR@MB
BET surface area (m^2/g)	0.3187	0.6080
BET total pore volume (cm^3/g)	0.000272	0.000479
BET pore size (nm)	3.41899	3.14962

3.1.5. Scanning electron microscopy

The morphology of TNR and TNR@MB as revealed by the SEM images shown in Fig. 5, can facilitate the adsorption of dyes, due to the irregular surface, thus making it possible to absorb and retain the dye molecules onto different parts of this material [26]. The heterogeneous rough and uneven surface with protuberances may provide an increase in the surface available for adsorption [7]. It is observed that the dye molecules are trapped inside some of the pores of the TNR.

3.2. Batch adsorption studies

3.2.1. Effect of pH on adsorption

The effect of pH on the adsorption of MB is presented in Fig. 6. It is observed that in a very acidic medium (pH = 2), the q_e could reach 5.7 with removal efficiency over 70%. As the pH increased from 2 to 4, there was a sharp rise in both the q_e and removal efficiency. Since MB is a cationic dye, it was expected that its adsorption should best take place at pH greater than the pH_{pzc}. Because at lower pH, the positively charged surface of the TNR would cause electrostatic repulsion of the MB, and the H^+ in solution would

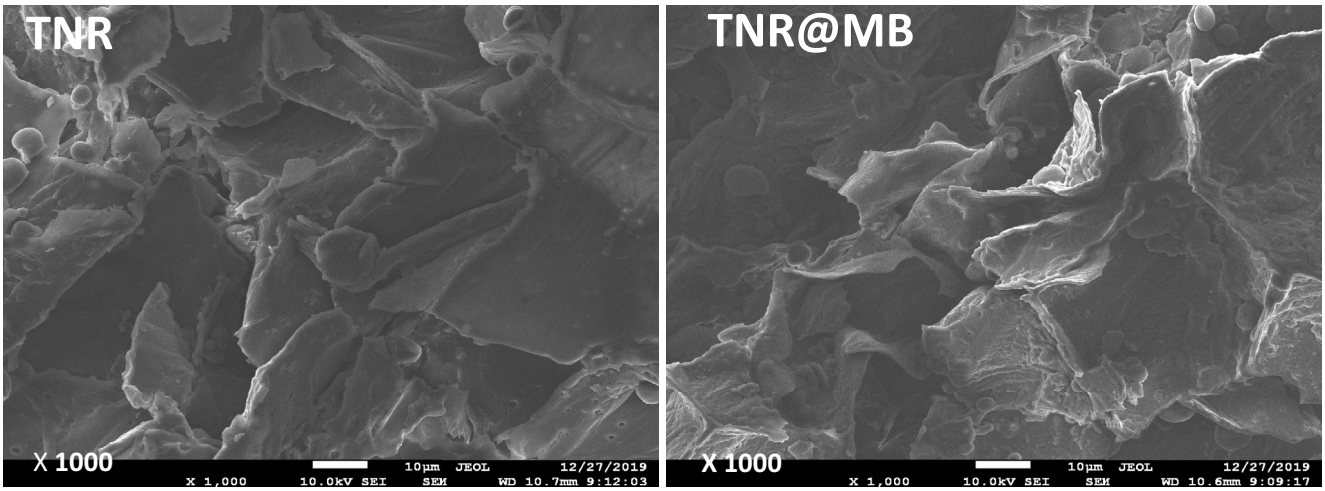

Fig. 5. SEM micrograph of TNR and TNR@MB.

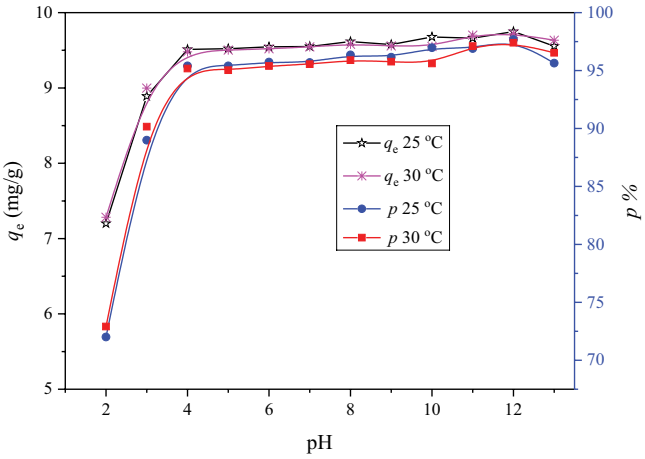

Fig. 6. Effect of pH on adsorption of MB at different temperatures (t = 6 h and C_0 = 100 mg/L).

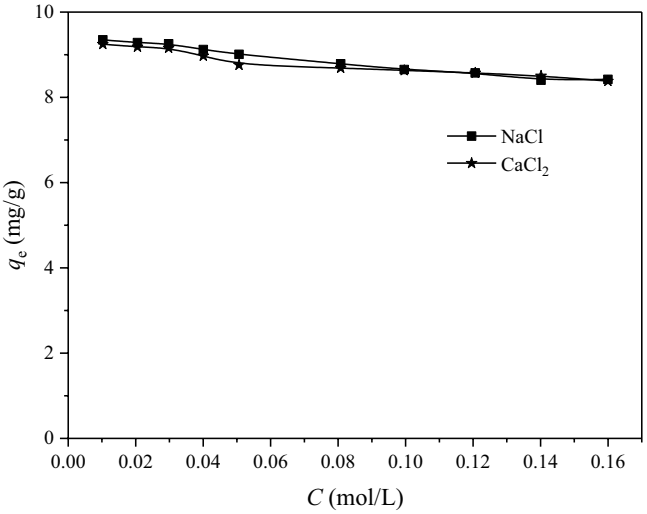

Fig. 7. Effects of salt concentration on adsorption (T = 30°C, pH = 4, t = 6 h, and C_0 = 100 mg/L).

also compete with MB for adsorption sites [4] on the TNR, hence relatively low adsorption would be expected at pH lower than 5.5. But Fig. 6 revealed that the adsorption process achieves equilibrium (over 95%) after pH 4. This can be explained by the fact that adsorption of MB onto the TNR was regulated by other factors in addition to ion exchange electrostatic force. For TNR to effectively remove MB in an acidic and basic medium is therefore reported for the first time. Subsequently, all other experiments were carried out at pH 4 to demonstrate the removal efficiency of TNR even in an acidic medium since most researchers report MB removal in an alkaline medium or neutral pH [1,14,15,27].

3.2.2. Effect of salt ion on adsorption of MB

The effect of various concentrations of NaCl and $CaCl_2$ solution on the amount of MB adsorbed onto per unit mass of TNR for an initial MB concentration of 100 mg/L is presented in Fig. 7. The effect of $CaCl_2$ was relatively more detrimental than that of NaCl. This observation is attributed to the ionic strength and charge density of Ca^{2+}, which is higher than that of Na^+. The decrease in q_e with increasing salt concentration as observed in Fig. 7 could be attributed to the competitive effect between MB ions and cations from the salt for the sites available for adsorption. The adsorption of MB was not significantly affected by the presence of salts as the q_e was over 8.3 even at a high salt concentration of 0.16 mol/L. These results implied that other actions, apart from ionic strength (such as hydrogen bond and Van der Waals' force), might have existed during the adsorption process. Hence, TNR can efficiently be used as a novel absorbent to remove MB from aqueous solutions with higher salt concentration.

3.2.3. Effect of adsorbent dose on the adsorption of MB by TNR

The influence of different adsorbent quantity on the removal of MB was investigated from 0.005 to 0.16 g.

As shown in Fig. 8, it can be observed that the removal efficiency of MB increased whiles the q_e decreased with an increasing dose of TNR due to the accessibility of higher adsorption sites. The percentage of removal increased from 68.2% to 96.5% when the adsorbent load increased from 0.01 to 0.2 g. With 0.1 g of the adsorbent dose, the maximum adsorption efficiency of 96.9% of MB was achieved, hence 0.1 g of the adsorbent dose was chosen as the optimal condition for the rest of the experiment. The primary factor explaining this observation is that the active adsorption sites remain unsaturated during the adsorption process, whereas the number of active sites available for adsorption increases by increasing the adsorbent dose. At higher dose concentration, there is a very fast superficial adsorption onto the TNR surface that produces a lower solute concentration in the solution than when the TNR dose is lower. Other researchers have documented similar observations [22,28].

3.2.4. Effect of contact time on adsorption

The effects of adsorption time (10 to 360 min) at different temperatures were investigated and the results are presented in Fig. 9. A two-stage kinetic behavior is evident from the graph. A very rapid initial adsorption occurred over a few minutes, which was followed by a longer period of much gradual adsorption at a slower uptake. The adsorbed quantity of MB onto per unit mass of TNR increased quickly, then after about 90 min, the change became slow as the adsorption reaction approached equilibrium with q_t of 9.40 mg/g.

This phenomenon could be explained by the fact that the adsorbents had abundant vacant adsorption sites at the initial stage, which enhanced the dye molecules to be absorbed by the adsorbent. With prolonged time, the mass of the dye molecules gradually occupied the active sites. The decrease in the available vacant adsorption sites resulted in a decrease in adsorption to reach the equilibrium state [4]. Adsorption quantity was not influenced significantly by temperature.

Removal of dye by adsorbent depends upon the interaction between the dye and adsorbent. Four kinetic models were applied to study and predict the possible dye adsorption mechanism as well as possible rates controlling steps [17]. These include the pseudo-first-order kinetic model (PFO), pseudo-second-order kinetic model (PSO), Elovich model, and intraparticle diffusion model (IPD).

The PFO kinetic model is represented by Eq. (3):

$$q_t = q_e\left(1 - e^{-k_1 t}\right) \tag{3}$$

where q_t (mg/g) is the adsorption capacity at time (t) and q_e (mg/g) is the adsorption capacity at equilibrium, k_1 (1/min) is the rate constant [29].

In the PSO model, the rate-limiting step is that of surface adsorption that involves chemisorption, where the removal of a pollutant from solution is due to physicochemical interactions between the absorbent and the absorbate. Its equation based on adsorption equilibrium capacity can be expressed in the form below (Eq. 4):

$$q_t = \frac{k_2 q_e^2 t}{1 + k_2 q_e t} \tag{4}$$

where q_t (mg/g) is the adsorption capacity at time (t) and q_e (mg/g) is the adsorption capacity at equilibrium, k_2 (g mg^{-1} min^{-1}) is the rate constant [29].

The Elovich equation is used for general application to chemisorption. The equation has been applied satisfactorily to some chemisorption processes and has been found to cover a wide range of slow adsorption rates. The same equation is often valid for systems in which the adsorbing surface is heterogeneous. The nonlinear form is expressed as:

$$q_t = \frac{\ln(\alpha\beta)}{\beta} + \frac{\ln t}{\beta} \tag{5}$$

where q_t is the quantity of adsorbate adsorbed at time t (mg/g), α is a constant related to chemisorption rate and β is a constant which depicts the extent of surface coverage [30].

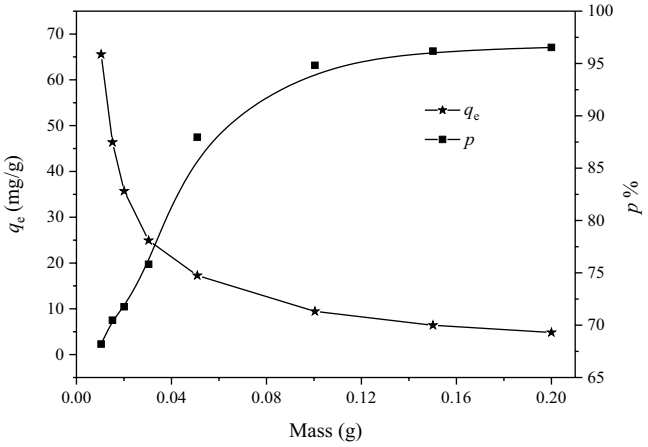

Fig. 8. Effect of adsorbent dose on adsorption (T = 30°C, pH = 4, t = 6 h, and C_0 = 100 mg/L).

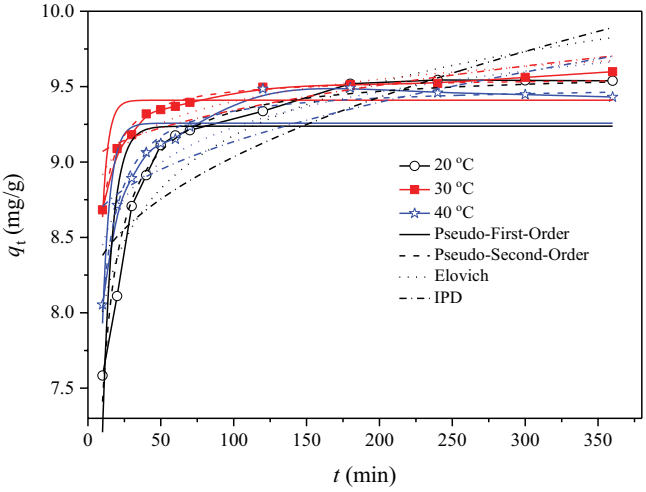

Fig. 9. Effect of contact time on adsorption and kinetic fitted curves (C_0 = 100 mg/L).

IPD based on the theory proposed by Weber and Morris [31] was used to describe the diffusion mechanism. Weber and Morris posited that the adsorbate uptake q_t varies almost proportionally with the square root of the contact time, $t^{1/2}$ and is expressed as follows:

$$q_t = k_t t^{1/2} + C \quad (6)$$

where k_t and C are the IPD rate constant (mg/g min$^{-1/2}$) and intercept, respectively. In the determination of which model best fit the experimental data, the R^2 is the most important determinant [32].

All parameters of these models were obtained using the nonlinear regressive analysis. The suitability of a model can be judged by the determined coefficient (R^2) and errors (SSE). The parameters of kinetic models were obtained and listed in Table 2. The fitted curves are also shown in Fig. 9. It was quite clear from the results of the kinetics models that the value of R^2 (Table 2) for PSO (0.971–0.983) for temperature 20°C, 30°C, and 40°C was higher than that obtained from Elovich equation (0.805–0.841), PFO (0.700–0.665) and IPD (0.636–0.579). Therefore, based on the value of R^2, it can be concluded that the PSO model is best fitted to the experimental data. In addition, another parameter that is considered alongside the R^2 is the errors (SSE). From Table 2, the SSE for PSO was the smallest (0.011–0.110) for the studied temperatures. Furthermore, the difference between values of q_e from the experimental data, $q_{e(\text{exp})}$, and the theoretical data, $q_{e(\text{theop})}$ was smaller at the same conditions. This showed that the PSO model could provide a more comprehensive reflection of the adsorption mechanism of MB onto TNR and effectively be used to predict the adsorption quantity. This observation also suggests that the adsorption is dependent on the amount of the solute adsorbed on the surface of the adsorbent and the number of active sites [4]. That notwithstanding, it is still difficult to illustrate the possible diffusion mechanism completely. Hence, the data from IPD model was also investigated.

With reference to Weber and Morris's theory, IPD controls the adsorption process if a plot of IPD is a straight line and all the intercepts are zero (passes through the origin). If it does not pass through the zero marks, then it is indicative of some degree of boundary layer control which further suggests that more than one diffusion mechanism is probably deciding the adsorption process [4]. From Table 2, all the intercepts of IPD are nonzero (C = 8.08–8.94), hence, the rate-limiting step is not associated with only IPD [32]. From the above, it is possible that many of the MB molecules diffuse into the small pores of the absorbent before being adsorbed, and that the adsorption rate simultaneously depends on the concentration of adsorbents and adsorbates [31].

Table 2
Parameters of kinetic models for MB adsorption

Kinetic	20°C	30°C	40°C
PFO			
$q_{e(\text{exp})}$ (mg/g)	9.54	9.60	9.43
$q_{e(\text{theop})}$ (mg/g)	9.24 ± 0.11	9.41 ± 0.050	9.26 ± 0.070
k_1	0.152 ± 0.020	0.250 ± 0.020	0.194 ± 0.020
R^2	0.670	0.665	0.700
SSE	1.27	0.222	0.534
PSO			
$q_{e(\text{exp})}$ (mg/g)	9.54	9.60	9.43
$q_{e(\text{theop})}$ (mg/g)	9.61 ± 0.045	9.57 ± 0.014	9.51 ± 0.025
k_2	0.0350 ± 0.0020	0.0990 ± 0.0040	0.0560 ± 0.0030
R^2	0.971	0.983	0.980
SSE	0.110	0.011	0.036
Elovich			
α	6.84 ± 0.30	8.43 ± 0.12	7.67 ± 0.22
β	0.508 ± 0.070	0.211 ± 0.030	0.340 ± 0.050
R^2	0.836	0.841	0.805
SSE	0.630	0.106	0.348
IPD			
k_t	0.096 ± 0.020	0.040 ± 0.010	0.0630 ± 0.020
C	8.08 ± 0.24	8.94 ± 0.10	8.51 ± 0.17
R^2	0.622	0.636	0.579
SSE	1.45	0.241	0.750

SSE = $\Sigma(q - q_c)^2$, q and q_c are the experimental value and calculated value according to the model, respectively.

3.2.4. Adsorption isotherms

The adsorption isotherm is presented in Fig. 10. The values of q_e increased with an increase in the equilibrium concentration, however, the temperature did not have any significant effect on adsorption quantity. To better understand the adsorption process, it is expedient to analyze the adsorption equilibrium parameters. Equilibrium isotherm equations are generally used to describe the experimental adsorption data [14]. An adsorption isotherm is characterized by certain constants whose values express the surface properties and affinity of the adsorbent and can also be used to find the adsorptive capacity of the adsorbent. In this paper, the Langmuir [33], Freundlich [34], Koble–Corrigan [35] and Temkin [36] models were applied.

The Langmuir model is used to describe the adsorption process of a monolayer on a uniform surface [33]. A basic assumption of the Langmuir theory is that sorption takes place at specific homogeneous sites within the adsorbent and that there is no interaction between molecules adsorbed on neighboring sides. Langmuir constant, q_m, represents the monolayer saturation at equilibrium. The other monocomponent Langmuir constant, K_L, indicates the affinity for the binding sites and energy of adsorption of MB. The value of K_L indicates to be either unfavourable ($K_L > 1$), linear ($K_L = 1$), favourable ($0 < K_L < 1$) and irreversible ($K_L = 0$). The saturated monolayer isotherm can be represented as:

$$q_e = \frac{q_m K_L C_e}{1 + K_L C_e} \tag{7}$$

The Freundlich model is an isothermal model describing the heterogeneous adsorption of multimolecular layers [34]. The Freundlich model does not provide information about maximum adsorption capacity and also do not describe the saturation behavior of the adsorbent [29]. The Freundlich isotherm is commonly presented as:

$$q_e = K_F C_e^{1/n} \tag{8}$$

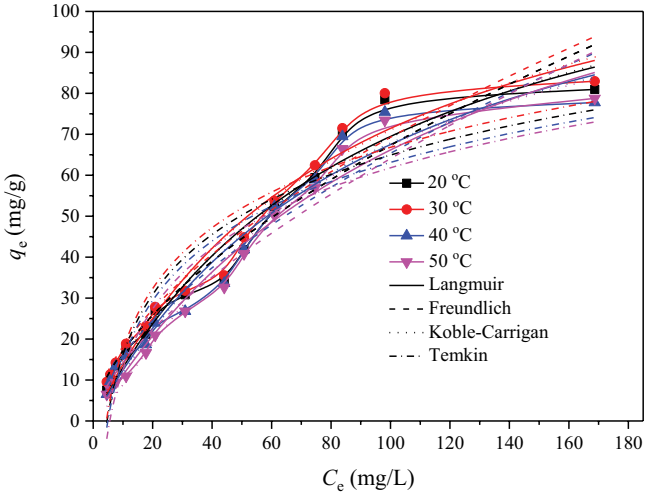

Fig. 10. Adsorption isotherms and fitted curves of MB adsorption onto TNR.

where K_F and n are Freundlich constants related to the adsorption capacity and adsorption intensity of the adsorbent. Using the two constants K_F and $1/n$, the properties of different adsorbents could be compared [9,29].

The Koble–Corrigan model is also a three-parameter equation for representing equilibrium adsorption data [35]. It is a combination of the Langmuir and Freundlich isotherm type models and is given by Eq. (9).

$$q_e = \frac{AC_e^n}{1 + BC_e^n} \tag{9}$$

where A, B, and n are the Koble–Corrigan parameters [35].

The Temkin isotherm was derived based on the assumption that the heat of adsorption of all molecules in the layer is linear rather than logarithmic, as implied in the Freundlich equation. This model is valid only for an intermediate range of ion concentrations [36]. The Temkin isotherm is given by:

$$q_e = A + B \ln C_e \tag{10}$$

where A and B are the two constants of the equation [29].

The fitted results from isotherms were presented in Table 3 and the fitted curves were also shown in Fig. 10. The data listed in Table 3 suggested that adsorption of MB onto TNR be guided by a complex system as the experimental data fitted relatively well into the Langmuir, Freundlich, and Koble–Corrigan equations. Temkin model was not a good fit from the experimental data, the heat of adsorption was not linear hence and the rising temperature was not beneficial for MB adsorption. From Table 3 the Freundlich parameters indicated easy uptake of MB by TNR ($0.1 < 1/n < 1$) [28]. This model fitting also suggested heterogeneous adsorption of multimolecular layers. The heterogeneous, rough, and uneven surface of the absorbent could be responsible for this. For Koble–Corrigan model, all the values of n were greater than 0.91 for all temperatures and this indicated that the isotherms were approaching the Langmuir form and at a high adsorbate concentration, this model reduces to Freundlich isotherm. However, at temperatures 40°C and 50°C, the n was greater than 1, which signified that the model was incapable of efficiently defining the experimental data [36].

Langmuir fitting suggests an electrostatic force of attraction mediating the dye removal. This could be explained by a large number of hydroxyl and carboxyl groups present on the TNR (Fig. 3) which is able to interact with the molecules of the dye. The Langmuir constant, q_m, represents the monolayer saturation at equilibrium. Also, the value of K_L was less than 1 indicating that the binding force was strong and that the adsorption was favorable. The values of q_m obtained at 20°C, 30°C, 40°C, and 50°C are 133, 133, 134 and 146 mg/g, respectively. The values of q_m about some adsorbent binding MB from the Langmuir constant are listed in Table 4. A comparison of maximum adsorption capacities and isotherm parameters of TNR and some other commercialized activated carbon for MB adsorption have been presented in Table 5. It is observed that almost all the commercially available activated carbons

Table 3
Parameters of isotherm models for MB adsorption

Isotherm	20°C	30°C	40°C	50°C
Langmuir				
$q_{e(\text{theop})}$ (mg/g)	133 ± 17	133 ± 15	134 ± 17	146 ± 17
K_L	0.011 ± 0.002	0.012 ± 0.002	0.010 ± 0.002	0.008 ± 0.002
R^2	0.957	0.960	0.958	0.973
SSE	329	316	316	216
Freundlich				
K_F	4.33 ± 0.10	4.78 ± 1.02	3.96 ± 1.01	3.14 ± 0.80
$1/n$	0.596 ± 0.05	0.581 ± 0.05	0.609 ± 0.06	0.655 ± 0.06
R^2	0.940	0.945	0.932	0.944
SSE	463	435	514	439
Koble–Corrigan				
A	1.69 ± 0.97	2.03 ± 1.06	1.06 ± 0.69	0.56 ± 0.33
B	0.012 ± 0.004	0.013 ± 0.004	0.009 ± 0.004	0.005 ± 0.002
n	0.949 ± 0.190	0.910 ± 0.180	1.08 ± 0.20	1.24 ± 0.17
R^2	0.954	0.957	0.955	0.975
SSE	327	308	312	183
Temkin				
A (–)	32.5 ± 7.3	31.9 ± 7.2	33.4 ± 7.3	36.8 ± 7.2
B	21.1 ± 2.0	21.4 ± 2.0	21.0 ± 2.1	22.1 ± 2.0
R^2	0.891	0.895	0.887	0.894
SSE	840	825	855	835

Table 4
MB adsorption by adsorbents: a selection of Langmuir constant, q_m, of various related substance from literature

Adsorbent	q_m (mg/g)	References
Phoenix tree's leaf	89.7	[14]
Cereal chaff	26.3	[15]
Modified sawdust	32.3	[37]
Giant duckweed	119	[38]
Rice husk	40.6	[27]
Cherry	39.8	[39]
Oak	29.9	[39]
Hazelnut	76.9	[39]
Walnut	59.2	[39]
Pitch-pine	27.8	[39]
Ficus carica bast	47.6	[40]
Water hyacinth root	185	[41]
Tiger nut residue	146	This work

present a higher Langmuir predicted adsorption capacities than that of TNR, however, these commercial activated carbons remain expensive, and their by-products after adsorption are not environmentally friendly, limiting their large application. Although the potential for TNR to be used as a green and cheap adsorbent for the removal of MB has been demonstrated, there are still some challenges that must be addressed in the future.

3.2.5. Thermodynamic parameters of adsorption

To opine the effect of temperature on the adsorption of MB onto TNR, thermodynamic parameters such as Gibb's free energy change ($\Delta G°$), enthalpy change ($\Delta H°$), and entropy change ($\Delta S°$) were calculated and examined as they also provide an insight into the adsorption mechanism and behavior [46]. The apparent equilibrium constant (K_c) of the adsorption is defined by the following expression;

$$K_c = \frac{C_{\text{ad,eq}}}{C_{\text{eq}}} \tag{11}$$

where $C_{\text{ad,eq}}$ (mg/L) is the concentration of MB on the adsorbent at equilibrium. The value of K_c can be obtained with the lowest experimental MB concentration. The value of K_c was used in the following equation to determine the Gibb's free energy of adsorption ($\Delta G°$).

$$\Delta G° = -RT \ln K_c^0 \tag{12}$$

The enthalpy ($\Delta H°$) and entropy ($\Delta S°$) can be obtained from the slope and intercept of van't Hoff equation of $\Delta G°$ vs. T:

$$\Delta G° = \Delta H° - T\Delta S° \tag{13}$$

where $\Delta G°$ (J) is standard Gibb's free energy change, R is the universal gas constant (8.314 J/mol K) and T (K) is the absolute temperature.

The thermodynamic parameters obtained according to Eqs. (11)–(13) are listed in Table 6. The negative values of $\Delta G°$ at all temperatures confirmed the spontaneous and irreversible nature of the adsorption processes [2]. Adsorption was not temperature-dependent as higher temperatures did not result in the linear decrease in the negative value of $\Delta G°$. The lower values of $\Delta G°$ showed that a physical process may largely mediate the adsorption process [2]. The negative value of $\Delta H°$ (–5.92 kJ/mol) confirmed that the reaction was exothermic, which is consistent with the observation that higher temperatures were not beneficial to the reaction. It has been reported that for adsorption to be mediated by physisorption, $\Delta H°$ must be smaller than 40 kJ/mol. Hence, we generally posit that the adsorption mechanism of MB to TNR is physisorption. The negative $\Delta S°$ value (–54.4 J/mol K) confirmed the decreased randomness at the solid-solute interface during adsorption and reflected the affinity of the adsorbent material for the dye [9]. The low value of $\Delta S°$ also indicates that no remarkable change in entropy occurs during the adsorption process. All the thermodynamic parameters mentioned above indicate that TNR can be used as a highly efficient adsorbent to remove MB from aqueous solution.

Table 6
Thermodynamic parameters of MB adsorption onto TNR

$\Delta H°$ (kJ/mol)	$\Delta S°$ (J/(mol K))	$\Delta G°$ (kJ/mol)			
		293 K	303 K	313 K	323 K
–5.92	–54.4	–7.26	–7.22	–8.01	–8.81

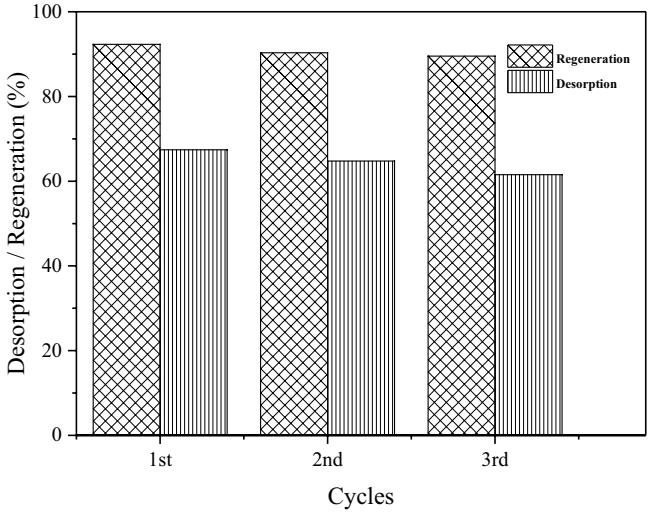

Fig. 11. Desorption and regeneration performance of TNR by 75% ethanol.

3.2.6. Regeneration and desorption

Regeneration of spent adsorbent and possible recovery of adsorbate will make the adsorption process economical and reduce environmental pollution [47–50]. The regeneration capacity of MB-loaded adsorbent was investigated in

Table 5
Comparison of maximum adsorption capacities from the Langmuir model and isotherm parameters of TNR and some other commercialized activated carbon materials for methylene blue adsorption

	Material	$q_{e(theop)}$ (mg/g)	Isotherm parameters						References
			pH	C_0 (mg/L)	T (°C)	Dose (g)	t (h)	V (mL)	
1	TNR	146.0	4.0	100	50	0.100	6	10	This work
2	BDH – Coconut-shell-based activated carbon supplied by Merck	522.2	10.0	12	30	0.005	400	200	[42]
3	F100 – Coal-based carbon from Calgon Corp.	533.9	10.0	12	30	0.005	400	200	[42]
4	BPL – Coal-based carbon obtained from Calgon Corp.	527.7	10.0	12	30	0.005	400	200	[42]
5	CAC – Commercial activated carbon supplied by E. Merck, India	980.3	7.4	600	30	2.000	2	50	[43]
6	NAPC – Natural activated plant-based carbon	15.43	3.0	200	25	0.500	5	50	[44]
7	F400 – Activated carbon produced by the gas activation of bituminous coal	476.0	9.0	800	20	0.050	7	50	[45]
8	PAC1 – Activated carbon produced from Venezuelan bituminous coal using physical activation	380.0	11.0	800	20	0.050	7	50	[45]
9	PAC2 – Activated carbon produced from New Zealand coal using steam activation	588.0	11.0	800	20	0.050	7	50	[45]

Natural activated plant-based carbon (NAPC)

batch mode. Desorption and regeneration efficiency using 75% ethanol as the desorption agent is shown in Fig. 11. The efficiency of desorption and regeneration was over 60% and 89% after three cycles respectively. This study shows that TNR can be used repeatedly without significantly losing its adsorption capacity for MB. The results indicate that following the successful adsorption of MB by TNR, the TNR may be recovered for consecutive uses with an advantage.

3.3. Cost analysis

TNR is readily available at no cost because it is an agricultural waste product. Nonetheless, the cost associated with collection and processing is estimated at 0.010 USD/kg. Comparing the cost of TNR with some commercially available adsorbents and activated carbons, it is very economical to use TNR. Hence, TNR offers an economic advantage over commercially available adsorbents and activated carbons.

4. Conclusion

TNR which is composed mainly of cellulose and lignin with more hydroxyl and carbonyl groups was studied as a potentially cheap and eco-friendly adsorbent for the removal of MB from solution. TNR was able to adsorb MB from aqueous solutions in a wide range of pH (acidic and alkaline mediums). The experimental results were analyzed by using the Langmuir, Freundlich, Koble–Corrigan and Temkin equations. Langmuir and Freundlich's equations suitably fitted the data. The maximum adsorption capacity as revealed by Langmuir isotherm was 146 mg/g. This present study showed that the adsorption rate simultaneously depends on the concentration of adsorbents and adsorbates. The kinetic process can be predicted by the PSO model. Thermodynamic analyses suggested that MB adsorption onto TNR was a physisorption process that was spontaneous and exothermic in nature and that no remarkable change in entropy occurred during the adsorption process. Regeneration was best achieved with 75% ethanol. The potential of TNR to be used as the future of green, reusable and sustainable adsorbent, particularly for the adsorption of organic dyes, has been evidenced, although further improvement is still required to enhance its adsorption capacity.

Acknowledgments

This work was supported in part by the National Natural Science Foundation of China (21205108, 21974125), the Foundation for University Key Teacher by Henan Province (2017GGJS007), and the Key Scientific Research Project in Universities of Henan Province (19A150048). The authors will like to express our gratitude to Wen Kang, Wan Huimin and Chen Shanshan for their assistance in the SEM and BET analysis.

References

[1] C. Nanthamathee, Effect of Co(II) dopant on the removal of methylene blue by a dense copper terephthalate, J. Environ. Sci., 81 (2019) 68–79.

[2] R. Ranjith, D. Maruthamuthu, S.P. Prabhavathi, P.S. Rajam, Enhanced adsorption and photocatalytic removal of cationic dyes in aqueous solutions by ternary graphene oxide-TiO_2–SiO_2 nanocomposites, J. Nanosci. Nanotechnol., 19 (2019) 5529–5545.

[3] C. Zhu, Y. Xia, Y. Zai, Y. Dai, X. Liu, J. Bian, Y. Liu, J. Liu, G. Li, Adsorption and desorption behaviors of HPEI and thermoresponsive HPEI based gels on anionic and cationic dyes, Chem. Eng. J., 369 (2019) 863–873.

[4] R. Wo, Q.L. Li, C. Zhu, Y. Zhang, G.F. Qiao, K.Y. Lei, P. Du, W. Jiang, Preparation and characterization of functionalized metal-organic frameworks with core/shell magnetic particles (Fe_3O_4@SiO_2@MOFs) for removal of Congo red and methylene blue from water solution, J. Chem. Eng. Data, 64 (2019) 2455–2463.

[5] Z. Huang, Y. Li, W. Chen, J. Shi, N. Zhang, X. Wang, Z. Li, L. Gao, Y.X. Zhang, Modified bentonite adsorption of organic pollutants of dye wastewater, Mater. Chem. Phys., 202 (2017) 266–276.

[6] L. Shen, Z. Jin, W. Xu, X. Jiang, Y.X. Shen, Y. Wang, Y. Lu, Enhanced treatment of anionic and cationic dyes in wastewater through live bacteria encapsulation using graphene hydrogel, Ind. Eng. Chem. Res., 58 (2019) 7817–7824.

[7] L. Meili, P.V.S. Lins, M.T. Costa, R.L. Almeida, A.K.S. Abud, J.I. Soletti, G.L. Dotto, E.H. Tanabe, L. Sellaoui, S.H.V. Carvalho, A. Erto, Adsorption of methylene blue on agroindustrial wastes: experimental investigation and phenomenological modelling, Prog. Biophys. Mol. Biol., 141 (2019) 60–71.

[8] S. Zhang, M. Zeng, J.X. Li, J. Li, J. Xu, X. Wang, Porous magnetic carbon sheets from biomass as an adsorbent for the fast removal of organic pollutants from aqueous solution, J. Mater. Chem. A, 2 (2014) 4391–4397.

[9] Y.F. Gu, M.M. Yang, W.L. Wang, R.P. Han, Phosphate adsorption from solution by zirconium-loaded carbon nanotubes in batch mode, J. Chem. Eng. Data, 64 (2019) 2849–2858.

[10] H. Zang, Y. Li, Y. Li, L. Chen, Q. Du, K. Zhou, H. Li, Y. Wang, L. Ci, Adsorptive removal of cationic dye from aqueous solution by graphene oxide/cellulose acetate composite, J. Nanosci. Nanotechnol., 19 (2019) 4535–4542.

[11] K. Saeed, M. Ishaq, S. Sultan, I. Ahmad, Removal of methyl violet 2-B from aqueous solutions using untreated and magnetite-impregnated almond shell as adsorbents, Desal. Water Treat., 57 (2016) 13484–13593.

[12] M. Ishaq, F. Javed, I. Amad, H. Ullah, Adsorption of crystal violet Dye from aqueous solutions onto low-cost untreated and NaOH treated almond shell, Iran. J. Chem. Chem. Eng., 35 (2016) 97–106.

[13] J.Y. Song, W.H. Zou, Y.Y. Bian, F.Y. Su, R.P. Han, Adsorption characteristics of methylene blue by peanut husk in batch and column modes, Desalination, 265 (2011) 119–125.

[14] R.P. Han, W.H. Zou, W.H. Yu, S.J. Cheng, Y.F. Wang, J. Shi, Biosorption of methylene blue from aqueous solution by fallen phoenix tree's leaves, J. Hazard. Mater., 141 (2007) 156–162.

[15] R.P. Han, Y.F. Wang, P. Han, J. Shi, J.J. Yang, Y.S. Lu, Removal of methylene blue from aqueous solution by chaff in batch mode, J. Hazard. Mater., 137 (2006) 550–557.

[16] W.L. Halvorson, Factsheet for *Cyperus esculentus L*, USGS Weeds in the West project: Status of Introduced Plants in Southern Arizona Parks, P. Guertin, Ed., US Geological Survey Southwest Biological Science Center Sonoran Desert Field Station, University of Arizona, Tucson, Arizona, 2003.

[17] J. Zhao, G. Liang, X. Zhang, X. Cai, R. Li, X. Xie, Z. Wang, Coating magnetic biochar with humic acid for high efficient removal of fluoroquinolone antibiotics in water, Sci. Total Environ., 688 (2019) 1205–1215.

[18] Y.Y. Su, B.L. Zhao, W. Xiao, R.P. Han, Adsorption behavior of light green anionic dye using cationic surfactant-modified wheat straw in batch and column mode, Environ. Sci. Pollut. Res., 20 (2013) 5558–5568.

[19] S. Srivastava, S.B. Agrawal, M.K. Mondal, Synthesis, characterization and application of *Lagerstroemia speciosa* embedded magnetic nanoparticle for Cr(VI) adsorption from aqueous solution, J. Environ. Sci., 55 (2017) 283–293.

[20] J. Shen, G. Huang, C. An, X. Xin, C. Huan, S. Rosendahl, Removal of Tetrabromobisphenol A by adsorption on pinecone-derived activated charcoals: synchrotron FTIR, kinetics and surface functionality analyses, Bioresour. Technol., 247 (2018) 812–820.
[21] O. Ao, N.B. Essien, U. Ra, Corn starch as a substitute for ccommercial food starch: FTIR and rheological characterization, J. Sci. Eng. Res., 3 (2016) 494–501.
[22] W. Zhou, X. Ge, D. Zhu, A. Langdon, L. Deng, Y. Hua, J. Zhao, Metal adsorption by quasi cellulose xanthogenates derived from aquatic and terrestrial plant materials, Bioresour. Technol., 102 (2011) 3629–3631.
[23] S. Rongpipi, D. Ye, E.D. Gomez, E.W. Gomez, Progress and opportunities in the characterization of cellulose – an important regulator of cell wall growth and mechanics, Front. Plant Sci., 9 (2019) 1–28.
[24] K. Kafle, R. Shi, C.M. Lee, A. Mittal, Y.B. Park, Y.H. Sun, S. Park, V. Chiang, S.H. Kim, Vibrational sum-frequency-generation (SFG) spectroscopy study of the structural assembly of cellulose microfibrils in reaction woods, Cellulose, 21 (2014) 2219–2231.
[25] Z. Liu, W. Yang, W. Xu, Y. Liu, Removal of elemental mercury by bio-chars derived from seaweed impregnated with potassium iodine, Chem. Eng. J., 339 (2018) 468–478.
[26] R.P. Han, L.J. Zhang, C. Song, M.M. Zhang, H.M. Zhu, L.J. Zhang, Characterization of modified wheat straw, kinetic and equilibrium study about copper ion and methylene blue adsorption in batch mode, Carbohydr. Polym., 79 (2010) 1140–1149.
[27] V. Vadivelan, K.V. Kumar, Equilibrium, kinetics, mechanism, and process design for the sorption of methylene blue onto rice husk, J. Colloid Interface Sci., 286 (2005) 90–100.
[28] Y.C. Rong, H. Li, L.H. Xiao, Q. Wang, Y.Y. Hu, S.S. Zhang, R.P. Han, Adsorption of malachite green dye from solution by magnetic activated carbon in batch mode, Desal. Water Treat., 106 (2018) 273–284.
[29] R.P. Han, J.J. Zhang, P. Han, Y.F. Wang, Z.H. Zhao, M.S. Tang, Study of equilibrium, kinetic and thermodynamic parameters about methylene blue adsorption onto natural zeolite, Chem. Eng. J., 145 (2009) 496–504.
[30] C. Aharoni, M. Ungarish, Kinetics of activated chemisorption. Part 1 – the non-elovichian part of the isotherm, J. Chem. Soc., Faraday Trans. 1 F, 72 (1976) 400–408.
[31] J.W. Weber, C. Morris, Kinetics of adsorption on carbon from solution, American Society of Civil Engineers, J. Sanit. Eng. Div., 89 (1963) 31–60.
[32] Saruchi, V. Kumar, Adsorption kinetics and isotherms for the removal of rhodamine B dye and Pb^{2+} ions from aqueous solutions by a hybrid ion-exchanger, Arabian J. Chem., 12 (2019) 316–329.
[33] I. Langmuir, The adsorption of gases on plane surfaces of glass, mica and platinum, J. Am. Chem. Soc., 40 (1918) 1361–1403.
[34] H.M.F. Freundlich, Over the adsorption in solution, J. Phys. Chem., 57 (1906) 358–471.
[35] R.A. Koble, T.E. Corrigan, Adsorption isotherms for pure hydrocarbons, Ind. Eng. Chem., 44 (1952) 383–387.
[36] N. Ayawei, A.N. Ebelegi, D. Wankasi, Modelling and interpretation of adsorption isotherms, J. Chem., 2017 (2017) 1–11, https://doi.org/10.1155/2017/3039817.
[37] D.S. De, J.K. Basu, Adsorption of methylene blue on to a low cost adsorbent developed from sawdust, Indian J. Environ. Prot., 19 (1998) 416–421.
[38] P. Waranusantigul, P. Pokethitiyook, M. Kruatrachue, E.S. Upatham, Kinetics of basic dye (methylene blue) biosorption by giant duckweed (*Spirodela polyrrhiza*), Environ. Pollut., 125 (2003) 385–392.
[39] F. Ferrero, Dye removal by low cost adsorbents: hazelnut shells in comparison with wood sawdust, J. Hazard. Mater., 142 (2007) 144–152.
[40] D. Pathania, S. Sharma, P. Singh, Removal of methylene blue by adsorption onto activated carbon developed from *Ficus carica* bast, Arabian J. Chem., 10 (2017) S1445–S1451.
[41] K.S. Low, C.K. Lee, K.K. Tan, Biosorption of basic dyes by water hyacinth roots, Bioresour. Technol., 52 (1995) 79–83.
[42] S. Wang, Z.H. Zhu, A. Coomes, F. Haghseresht, G.Q. Lu, The physical and surface chemical characteristics of activated carbons and the adsorption of methylene blue from wastewater, J. Colloid Interface Sci., 284 (2005) 440–446.
[43] N. Kannan, M.M. Sundaram, Kinetics and mechanism of removal of methylene blue by adsorption on various carbons - a comparative study, Dyes Pigm., 51 (2001) 25–40.
[44] A. Moldovan, E. Neag, V. Băbălău-Fuss, O. Cadar, V. Micle, C. Roman, Optimized removal of methylene blue from aqueous solution using a commercial natural cctivated plant-based carbon and Taguchi experimental design, Anal. Lett., 52 (2019) 150–162.
[45] E.N. El Qada, S.J. Allen, G.M. Walker, Adsorption of basic dyes from aqueous solution onto activated carbons, Chem. Eng. J., 135 (2008) 174–184.
[46] R.D. Zhang, J.H. Zhang, X.N. Zhang, C.C. Dou, R.P. Han, Adsorption of Congo red from aqueous solutions using cationic surfactant modified wheat straw in batch mode: kinetic and equilibrium study, J. Taiwan Inst. Chem. Eng., 45 (2014) 2578–2583.
[47] Y.C. Rong, R.P. Han, Adsorption of *p*-chlorophenol and *p*-nitrophenol in single and binary systems from solution using magnetic activated carbon, Korean J. Chem. Eng., 36 (2019) 942–953.
[48] B.L. Zhao, W. Xiao, Y. Shang, H.M. Zhu, R.P. Han, Adsorption of light green anionic dye using cationic surfactant-modified peanut husk in batch mode, Arabian J. Chem., 10 (2017) S3595–S3602.
[49] T. Zhou, W.Z. Lu, L.F. Liu, H.M. Zhu, Y.B. Jiao, S.S. Zhang, R.P. Han, Effective adsorption of light green anionic dye from solution by CPB modified peanut in column mode, J. Mol. Liq., 211 (2015) 909–914.
[50] M.Y. Liu, J.J. Dong, W.L. Wang, M.M. Yang, Y.F. Gu, R.P. Han, Study of methylene mlue adsorption from solution by magnetic graphene oxide composites, Desal. Water Treat., 147 (2019) 398–408.